Article

Influences of Fracturing Fluid Injection on Mechanical Integrity of Cement Sheath under Four Failure Modes

Honglin Xu [1], Tianshou Ma [2,3,](#)* , Nian Peng [1,2] and Bin Yang [1]

[1] School of Petroleum and Natural Gas Engineering, Chongqing University of Science and Technology, Chongqing 401331, China; 2015009@cqust.edu.cn (H.X.); 201721000573@stu.swpu.edu.cn (N.P.); 2009065@cqust.edu.cn (B.Y.)

[2] State Key Laboratory of Oil and Gas Reservoir Geology and Exploitation, Southwest Petroleum University, Chengdu 610500, China

[3] State Key Laboratory of Geomechanics and Geotechnical Engineering, Institute of Rock and Soil Mechanics, Chinese Academy of Sciences (CAS), Wuhan 430071, China

* Correspondence: matianshou@swpu.edu.cn; Tel.: +86-28-8303-2458

check for updates

Abstract: The significant decreased wellbore temperature and increased casing pressure during fracturing fluid injection present a big challenge for the mechanical integrity of cement sheath in fracturing wells. Based on the theories of elastic mechanics, thermodynamics, and a multi-layer composed thick-wall cylinder, this paper proposed a new mechanical model of cement sheath for fracturing wells, coupling pressure, and thermal loads, which consider the failure modes of de-bonding, radial cracking, disking, and shear failure. The radial nonuniform temperature change and the continuous radial stress and radial displacement at two interfaces have been considered. With the proposed model, the radial distributions of failure stress and the corresponding safety factor for cement sheath during fracturing fluid injection have been analyzed and compared under four failure modes. Results show that the decreased wellbore temperature will produce significant tri-axial tensile stress and induce cement failure of de-bonding, radial cracking, and disking. The increased casing pressure will significantly lower the risk of de-bonding but also aggravate radial cracking and shear failure. For integrity protection of cement sheath, increasing the injected fluid temperature, maintaining higher circulation pumping pressures, and adopting cement sheath with a low elasticity modulus have been suggested for fracturing wells.

Keywords: cement sheath; analytical model; failure stress; safety factor; fracturing wells

1. Introduction

For maintaining gas well's long-term and safe production, mechanical integrity of cement sheath has been given more emphasis in recent years. Field experiences and laboratory studies have both proven that cement sheath is very likely to fail after downhole operations, such as pressure testing, hydraulic fracturing, acidizing, steam injection, and more [1–3]. The cement sheath fails mainly because of the loads from variations of wellbore temperature and pressure. For fracturing wells, because of the high displacement and pump pressure fracturing fluid injection into wellbore, the wellbore temperature decrease (by $-70\,^{\circ}$C) and casing pressure increase (by 70 MPa) are both very serious. In addition, this leads to cement sheath failure and continuous annular casing pressure. Presently, Portland cement is still frequently-used for wellbore purposes. However, because of its high elasticity and lower tensile strength, it is more likely to fail. Consequently, an analysis of the

failure stress and the corresponding failure mode in the cement sheath during the fracturing process is significant for the wellbore safety of fracturing wells.

Currently, some theoretical mechanical models of cement sheath coupling pressure and temperature loads have been established for high pressure and high temperature (HPHT) gas wells and steam injecting wells. Thiercelin et al. [4] first proposed the mechanical model for the cement sheath in which the influence of thermo-elastic properties of materials on cement failure was verified. Li et al. [5] proposed a thermal stress model for a coupled casing-cement-formation system in a thermal well and investigated the casing failure behaviors. After that Li et al. [6] further established a mechanical model of cement sheath coupling the effects of temperature and pressure loads in a non-uniform in-situ stress field. Bois et al. [7] also proposed a cement sheath model. The failure modes were analyzed by investigating the casing deformation induced by wellbore temperature variation. Haider et al. [8] developed a composite axisymmetric casing-cement-formation model for a CO_2 storage well. The results indicated that the decrease in wellbore temperature could induce radial tensile stress in the cement sheath. Bui et al. [9] also presented a mechanical model for cement failure prediction, where the non-uniform stress field and the thermal stress were involved. Xi et al. [10] established a transient thermo-mechanical model of casing-cement sheath-formation assembly by using the analytical method and the numerical method comprehensively. Our previous study [11] proposed a mechanical model of casing-cement-formation system and investigated the influence of wellhead casing pressure on cement sheath integrity for HPHT gas wells. After that, we further proposed a model of thermal stress for cement sheath during hydraulic fracturing [12], where radial non-uniform temperature change was involved, and the main influencing factors were also investigated. All the models mentioned above could be used to simulate the stress and failure of cement sheath in some ways. However, because of the complexity of wellbore geometry and the diversity of cement sheath failure modes, the present models cannot provide a relatively accurate and comprehensive failure analysis for cement sheath.

In this paper, a new mechanical model of cement sheath, coupling pressure, and thermal loads and considering the failure modes of de-bonding, radial cracking, disking, and shear failure, has been proposed for fracturing wells, based on the elastic mechanics, thermodynamics theory, and the theory of multi-layer composed thick-wall cylinder. The radial non-uniform temperature change in the combined system has been considered and both the radial stress and radial displacement at the casing-cement sheath interface and the cement sheath-formation interface are supposed to be continuous. Based on the proposed model, the radial distributions of failure stress and corresponding safety factor for cement sheath during fracturing fluid injection have been analyzed and compared under four failure modes. In addition, some measures have been proposed for cement sheath protection, which can be of great significance for decreasing the risk of sustained casing pressure after fracturing operations.

2. Mechanical Model Development and Solution

2.1. Basic Assumptions

To maintain the wellbore mechanical and hydraulic integrity during fracturing and long-term production, the open hole is usually cemented with a steel casing. When the high pump pressure fluid with continuous large displacement is injected into the wellbore, the coupled loads from increased casing pressure p_i and decreased wellbore temperature $T(r)$ will simultaneously exert on the casing-cement sheath-formation combined system, which induces cement sheath stresses. The schematic diagram of the casing-cement-formation combined system during fracturing fluid injection is shown in Figure 1. Before developing the mechanical model of cement sheath, to make the present model tractable, the following assumptions are made [11,12].

(1) The casing, cement sheath, and formation are continuous, homogeneous, and isotropic.
(2) The casing-cement sheath-formation system is completely cemented and axisymmetric.

(3)   Both casing-cement sheath and cement sheath-formation interface satisfy the continuity conditions for radial stress and radial displacement.

(4)   The radial non-uniform temperature varies along the combined casing-cement sheath -formation system except for casing as consideration of its thin wall and well heat conduction performance.

(5)   The temperature at the inner wall of casing is equal to the wellbore fracturing fluid temperature and that at the outer wall of formation maintains an original formation temperature during fracturing.
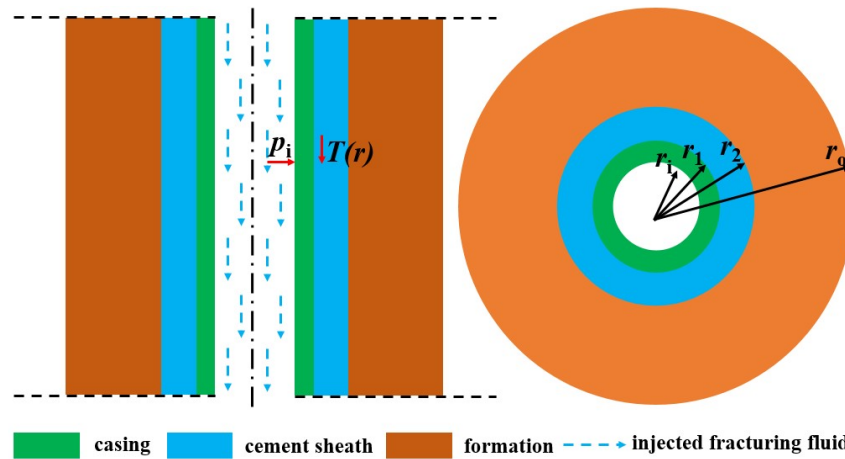
Figure 1. The schematic diagram of casing-cement sheath-formation combined system during fracturing fluid injection.

2.2. Cement Sheath Stress Induced by the Decrease of Wellbore Temperature

The continuous fracturing fluid injection will significantly decrease wellbore temperature and constrict the combined system, which will lead to thermal stresses in the cement sheath. Our previous study investigated thermal stresses for cement sheath during hydraulic fracturing based on the elastic mechanics and thermodynamics theory [13], and the general solutions of radial thermal displacement and thermal stresses for thick wall cylinder were given as follows [12,13].

$$
\begin{cases}
u^T = \frac{1+\mu}{1-\mu}\frac{\alpha}{r}\int_a^r T(r)rdr + C_1 r + \frac{C_2}{r} \\
\sigma_r^T = -\frac{\alpha E}{1-\mu}\frac{1}{r^2}\int_a^r T(r)rdr + \frac{E}{1+\mu}\left(\frac{C_1}{1-2\mu} - \frac{C_2}{r^2}\right) \\
\sigma_\theta^T = \frac{\alpha E}{1-\mu}\frac{1}{r^2}\int_a^r T(r)rdr - \frac{\alpha E T_b(r)}{1-\mu} + \frac{E}{1+\mu}\left(\frac{C_1}{1-2\mu} + \frac{C_2}{r^2}\right) \\
\sigma_z^T = -\frac{\alpha E T(r)}{1-\mu} + \frac{2\mu E C_1}{(1+\mu)(1-2\mu)}
\end{cases}
\tag{1}
$$

In Equation (1), $T(r)$ stands for the radial temperature change at radius of r in the cylinder after and before fracturing fluid injection. Considering wellbore temperature varies radially constant in casing and logarithmically in cement sheath and formation, if the temperature at the inner boundary of casing is T_i before fracturing and it decreased to T_t after fracturing fluid injection, while the temperature at the outer boundary of formation is constantly T_e, the radial wellbore temperature change $T(r)$ can be determined by the following [12].

$$
T(r) = \begin{cases}
T_t - T_i & (r_i \leq r \leq r_1) \\
T_t - T_i + (T_i - T_t)\frac{\ln(r/r_1)}{\ln(r_o/r_1)} & (r_1 \leq r \leq r_o)
\end{cases}
\tag{2}
$$

For the integral expression $\int_a^r T(r)rdr$ in Equation (1), it can be deduced as:

$$\int_a^r T(r)rdr = \begin{cases} \frac{1}{2}(T_t - T_i)(r^2 - r_i^2) & (r_i \le r \le r_1) \\ \frac{1}{2}(T_t - T_i)(r^2 - r_1^2) + \frac{(T_i - T_t)}{2\ln(r_o/r_1)}\left[r^2 \ln\left(\frac{r}{r_1}\right) - \frac{r^2}{2} + \frac{r_1^2}{2}\right] & (r_1 \le r \le r_o) \end{cases} \tag{3}$$

Submitting Equations (2) and (3) into Equation (1), the thermal radial displacement and thermal stresses for combined system can be determined, and the detailed derivative results are shown in Appendix A.

2.3. Cement Sheath Stresses Induced by the Increase of Casing Pressure

Taking wellbore temperature as no change during fracturing fluid injection and, since only the increased casing pressure acts on the casing-cement sheath-formation combined system, casing expansion and induced stresses in the cement sheath will occur. Assuming the plane strain of the combined system ($\varepsilon_z \approx 0$), the following can be obtained [13].

$$\sigma_z^P = \mu\left(\sigma_r^P + \sigma_\theta^P\right) \tag{4}$$

Furthermore, the radial displacement of a cylinder induced by the increased inner pressure can be expressed below.

$$u^P = \frac{r}{E}\left[\left(1 - \mu^2\right)\sigma_\theta^P - \left(\mu + \mu^2\right)\sigma_r^P\right] \tag{5}$$

If the contact pressure induced by increased casing pressure is p_{c1} at the casing-cement sheath interface and p_{c2} at the cement sheath-formation interface respectively, the induced stress in the cement sheath can be calculated with the Lame Formula [13]. Now, we will solve p_{c1} and p_{c2} with the interfacial continuity conditions.

For the casing, because it is subjected to the increased casing pressure p_i at its inner wall and the contact pressure p_{c1} at its outer wall, its radial and tangential stresses can be obtained with the Lame Formula as follows:

$$\begin{cases} \sigma_{rs}^P = \frac{p_i r_i^2}{r_1^2 - r_i^2}\left(1 - \frac{r_1^2}{r^2}\right) - \frac{p_{c1} r_1^2}{r_1^2 - r_i^2}\left(1 - \frac{r_i^2}{r^2}\right) \\ \sigma_{\theta s}^P = \frac{p_i r_i^2}{r_1^2 - r_i^2}\left(1 + \frac{r_1^2}{r^2}\right) - \frac{p_{c1} r_1^2}{r_1^2 - r_i^2}\left(1 + \frac{r_i^2}{r^2}\right) \end{cases} \tag{6}$$

By submitting Equation (6) into Equation (5), the radial displacement of the casing at its outer wall ($r = r_1$) can be obtained.

$$u_s^P|_{r=r_1} = \frac{r_1}{E_s}\left[\left(1 - \mu_s^2\right)\left(\frac{2r_i^2}{r_1^2 - r_i^2}p_i - \frac{r_1^2 + r_i^2}{r_1^2 - r_i^2}p_{c1}\right) + \left(\mu_s + \mu_s^2\right)p_{c1}\right] \tag{7}$$

For the cement sheath, because it is subjected to the contact pressure p_{c1} at its inner wall and the contact pressure p_{c2} at its outer wall, its radial and tangential stresses can also be obtained with the Lame Formula below.

$$\begin{cases} \sigma_{rc}^P = \frac{p_{c1} r_1^2}{r_2^2 - r_1^2}\left(1 - \frac{r_2^2}{r^2}\right) - \frac{p_{c2} r_2^2}{r_2^2 - r_1^2}\left(1 - \frac{r_1^2}{r^2}\right) \\ \sigma_{\theta c}^P = \frac{p_{c1} r_1^2}{r_2^2 - r_1^2}\left(1 + \frac{r_2^2}{r^2}\right) - \frac{p_{c2} r_2^2}{r_2^2 - r_1^2}\left(1 + \frac{r_1^2}{r^2}\right) \end{cases} \tag{8}$$

By submitting Equation (8) into Equation (5), the radial displacement of the cement sheath at its inner wall ($r = r_1$) can be obtained.

$$u_c^P|_{r=r_1} = \frac{r_1}{E_c}\left[\left(1 - \mu_c^2\right)\left(\frac{r_2^2 + r_1^2}{r_2^2 - r_1^2}p_{c1} - \frac{2r_2^2}{r_2^2 - r_1^2}p_{c2}\right) + \left(\mu_c + \mu_c^2\right)p_{c1}\right] \tag{9}$$

According to the continuity condition at the casing-cement sheath interface, there exists $u_s^P|_{r=r_1} = u_c^P|_{r=r_1}$. Thus, we can get the following.

$$
\begin{aligned}
&\left[E_c\left(\mu_s + \mu_s{}^2\right) - \frac{r_1^2 + r_i^2}{r_1^2 - r_i^2} E_c\left(1 - \mu_s{}^2\right) - \frac{r_2^2 + r_1^2}{r_2^2 - r_1^2} E_s\left(1 - \mu_c{}^2\right) - E_s\left(\mu_c + \mu_c{}^2\right) \right] p_{c1} \\
&+ \frac{2r_2^2}{r_2^2 - r_1^2} E_s\left(1 - \mu_c{}^2\right) p_{c2} = -\frac{2r_i^2}{r_1^2 - r_i^2} E_c\left(1 - \mu_s{}^2\right) p_i
\end{aligned}
\tag{10}
$$

Similarly, the radial displacement of the cement sheath at its outer wall ($r = r_2$) can also be obtained as follows.

$$
u_c^P|_{r=r_2} = \frac{r_2}{E_c} \left[\left(1 - \mu_c{}^2\right) \left(\frac{2r_1^2}{r_2^2 - r_1^2} p_{c1} - \frac{r_2^2 + r_1^2}{r_2^2 - r_1^2} p_{c2} \right) + \left(\mu_c + \mu_c{}^2\right) p_{c2} \right]
\tag{11}
$$

For the formation, because it is subjected to the contact pressure p_{c2} at its inner wall and the changed formation pressure p_f at its outer wall, its radial and tangential stresses can also be obtained with the Lame Formula below.

$$
\begin{cases}
\sigma_{rf}^P = \dfrac{p_{c2}r_2^2}{r_o^2 - r_2^2}\left(1 - \dfrac{r_o^2}{r^2}\right) - \dfrac{p_f r_o^2}{r_o^2 - r_2^2}\left(1 - \dfrac{r_2^2}{r^2}\right) \\[2mm]
\sigma_{\theta f}^P = \dfrac{p_{c2}r_2^2}{r_o^2 - r_2^2}\left(1 + \dfrac{r_o^2}{r^2}\right) - \dfrac{p_f r_o^2}{r_o^2 - r_2^2}\left(1 + \dfrac{r_2^2}{r^2}\right)
\end{cases}
\tag{12}
$$

Then, by submitting Equation (12) into Equation (5), the radial displacement of the formation at its inner wall ($r = r_2$) can be obtained.

$$
u_f^P|_{r=r_2} = \frac{r_2}{E_f} \left[\left(1 - \mu_f{}^2\right) \left(\frac{r_o^2 + r_2^2}{r_o^2 - r_2^2} p_{c2} - \frac{2r_o^2}{r_o^2 - r_2^2} p_f \right) + p_{c2}\left(\mu_f + \mu_f{}^2\right) \right]
\tag{13}
$$

According to the continuity condition at the cement sheath-formation interface, there exists $u_c^P|_{r=r_2} = u_f^P|_{r=r_2}$. Thus, we can get the following.

$$
\begin{aligned}
&\left[E_f\left(\mu_c + \mu_c{}^2\right) - \frac{r_2^2 + r_1^2}{r_2^2 - r_1^2} E_f\left(1 - \mu_c{}^2\right) - \frac{r_o^2 + r_2^2}{r_o^2 - r_2^2} E_c\left(1 - \mu_f{}^2\right) - E_c\left(\mu_f + \mu_f{}^2\right) \right] p_{c2} \\
&+ \frac{2r_1^2}{r_2^2 - r_1^2} E_f\left(1 - \mu_c{}^2\right) p_{c1} = -\frac{2r_o^2}{r_o^2 - r_2^2} E_c\left(1 - \mu_f{}^2\right) p_f
\end{aligned}
\tag{14}
$$

Solving Equations (10) and (14) simultaneously, the contact pressure p_{c1} and p_{c2} can be obtained. Lastly, from Equation (8) we can easily get the radial stress σ_{rc}^P and tangential stress $\sigma_{\theta c}^P$ respectively. Furthermore, the axial stress σ_{zc}^P in the cement sheath caused by the increased casing pressure can be calculated by Equation (4) as:

$$
\sigma_{zc}^P = \mu_c\left(\sigma_{rc}^P + \sigma_{\theta c}^P\right)
\tag{15}
$$

2.4. Combined Stresses of Cement Sheath during Fracturing Fluid Injection

In fact, the cement sheath will simultaneously suffer from induced stresses caused by decreased wellbore temperature and increased casing pressure during the fracturing fluid injection. Therefore, the combined radial, tangential, and axial stress of cement sheath during fracturing fluid injection can be expressed as follows.

$$
\begin{cases}
\sigma_{rc} = \sigma_{rc}^T + \sigma_{rc}^P \\
\sigma_{\theta c} = \sigma_{\theta c}^T + \sigma_{\theta c}^P \\
\sigma_{zc} = \sigma_{zc}^T + \sigma_{zc}^P
\end{cases}
\tag{16}
$$

2.5. Failure Criterion and Safety Factor for Cement Sheath

Four kinds of failure modes may lead to the loss of zonal isolation for cement sheath including inner debonding, outer debonding, radial cracking, shear damage, and disking. Bois et al. [14] illustrated that in Figure 2. Debonding, radial cracking, and disking can be determined with the maximum tensile stress criterion, while shear failure can be determined with the Mohr-Coulomb Criterion or the Mogi-Coulomb Criterion. Compared to the Mogi-Coulomb Criterion, because the Mohr-Coulomb Criterion does not consider the effect of intermediate principal stress on the strength of the material, it cannot reflect the real failure under a true tri-axial stress state in the rock [15,16]. The Mogi-Coulomb Criterion was selected in the paper.

| casing | cement sheath | formation | failure surface |

(**a**)   (**b**)   (**c**)   (**d**)   (**e**)
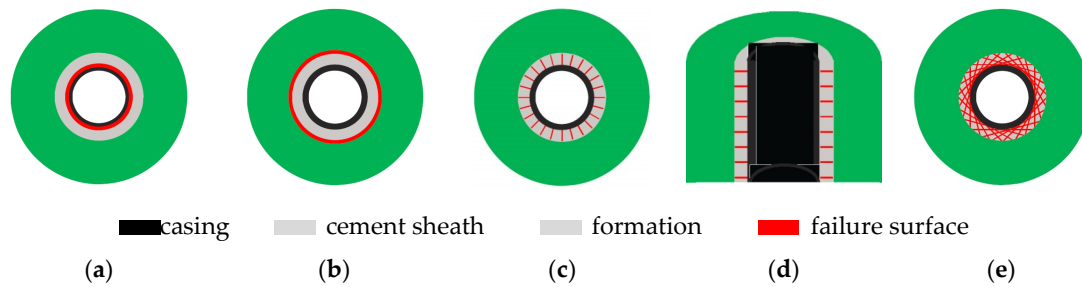
Figure 2. Failure modes in the cement sheath. (**a**) Inner de-bonding; (**b**) Outer de-bonding; (**c**) Radial cracking; (**d**) Disking; (**e**) Shear damage.

If the radial tensile stress at the casing-cement sheath interface or the cement sheath-formation interface exceeds the tensile strength of cement sheath, the de-bonding failure can be described as follows [17].

$$\sigma_{rc}|_{r=r_1\ or\ r_2} > \sigma_{tc} \tag{17}$$

If the tangential tensile stress in the cement sheath surpasses its tensile strength, cracking will begin to form and propagate along the radial direction. When multiple radial cracking are linked, the leakage path can be generated. The radial cracking failure can be expressed by Equation (18) below.

$$\sigma_{\theta c} > \sigma_{tc} \tag{18}$$

Similarly, if the axial tensile stress in the cement sheath exceeds its tensile strength, disking will begin to form and run across the cement wall. The disking failure can be described below.

$$\sigma_{zc} > \sigma_{tc} \tag{19}$$

Shear failure is a critical failure mode, which typically causes an entire failure for cement sheath. The Mogi-Coulomb Criterion assumes that shear failure will occur when the octahedral shear stress τ_{oct} in the cement sheath exceeds the maximum allowable shear stress $\tau_{c\max}$, which can be expressed as the following equation [15,16].

$$\frac{1}{3}\sqrt{(\sigma_{rc} - \sigma_{\theta c})^2 + (\sigma_{rc} - \sigma_{zc})^2 + (\sigma_{\theta c} - \sigma_{zc})^2} = \tau_{oct} > \tau_{c\max} \tag{20}$$

If a linear form is considered for the Mogi-Coulomb criterion and, noting that the compressive stress is negative in this paper, the maximum allowable shear stress $\tau_{c\max}$ in Equation (20) can be determined by the equation below [18].

$$\tau_{c\max} = c_c \cos\phi_c - \frac{\sigma_1 + \sigma_3}{2}\sin\phi_c \tag{21}$$

Considering the following relationship between the uniaxial compressive strength of cement sheath σ_{cc} and its cohesion c_c, the internal friction angle ϕ_c is shown below.

$$\sigma_{cc} = 2c_c \frac{\cos \phi_c}{1 - \sin \phi_c} \tag{22}$$

If σ_{cc} and ϕ_c are both known, by combining Equations (20)–(22), we can express the Mogi-Coulomb Criterion below.

$$\frac{1}{3} \sqrt{(\sigma_{rc} - \sigma_{\theta c})^2 + (\sigma_{rc} - \sigma_{zc})^2 + (\sigma_{\theta c} - \sigma_{zc})^2} > \frac{1 - \sin \phi_c}{2} \sigma_{cc} - \sin \phi_c \frac{\sigma_1 + \sigma_3}{2} \tag{23}$$

According to the failure criteria above, the safety factors for four failure modes can be calculated respectively, as shown in Table 1.

Table 1. Safety factor for cement sheath.

Failure Mode	Failure Criterion	Safety factor (*SF*)
Inner de-bonding	$\sigma_{rc}\|_{r=r_1} > \sigma_{tc}$	$SF = \sigma_{tc}/\sigma_{rc}\|_{r=r_1}$
Outer de-bonding	$\sigma_{rc}\|_{r=r_2} > \sigma_{tc}$	$SF = \sigma_{tc}/\sigma_{rc}\|_{r=r_2}$
Radial cracking	$\sigma_{\theta c} > \sigma_{tc}$	$SF = \sigma_{tc}/\sigma_{\theta c}$
Disking	$\sigma_{zc} > \sigma_{tc}$	$SF = \sigma_{tc}/\sigma_{zc}$
Shear failure	$\tau_{oct} > \tau_{cmax}$	$SF = \tau_{cmax}/\tau_{oct}$

3. Mechanical Integrity Analysis of Cement Sheath during Fracturing Fluid Injection

3.1. Basic Calculation Parameters

A shale gas fracturing well in the Sichuan Basin in China was selected for the analysis of mechanical integrity of cement sheath during fracturing fluid injection. The 215.9 mm open hole was cemented with 139.7 mm × 9.17 mm P110 casing. The basic calculation parameters, including wellbore geometry parameters, material property parameters, and operation parameters, are listed in Table 2.

**Table 2.** Basic calculation parameters.

No.	Symbol	Value	Unite	No.	Symbol	Value	Unit
1	r_i	60.68	mm	11	μ_s	0.30	dimensionless
2	r_1	69.85	mm	12	μ_c	0.19	dimensionless
3	r_2	107.95	mm	13	μ_f	0.21	dimensionless
4	r_o	1079.5	mm	14	T_i	100	°C
5	α_s	1.15×10^{-5}	1/°C	15	T_t	30–70	°C
6	α_c	1.03×10^{-5}	1/°C	16	T_e	100	°C
7	α_f	1.03×10^{-5}	1/°C	17	p_i	0–70	MPa
8	E_s	206	GPa	18	σ_{tc}	2.3	MPa
9	E_c	10	GPa	19	σ_{cc}	32	MPa
10	E_f	30	GPa	20	φ_c	30	°

3.2. Results and Discussion

To make clear the failure laws of cement shear during fracturing fluid injection, the proposed cement sheath stress model has been validated by the FEA method and then the corresponding failure stresses and safety factors of cement sheath under a different failure mode have been calculated according to the basic parameters in Table 2. Simultaneously, when seeking the measures of protecting cement sheath, the safety factors have also been investigated under a different elasticity modulus of the cement sheath E_c.

3.2.1. Cement Sheath Stresses Validated by the FEA Method

Up to now, as the complexity of the casing-cement sheath-formation combined system and the difficulty of applying coupled loads, fewer experimental studies were conducted about the in situ cement sheath integrity during fracturing. To validate the cement sheath stress model proposed in this paper, a 2D axisymmetric casing-cement sheath-formation model has been established with Ansys Workbench 14.5. Figure 3 shows the finite element analysis model of casing-cement sheath-formation combined system and the element type of Plane 183 was selected for this analysis. For simulating cement sheath stresses induced by increased casing pressure and decreased wellbore temperature during fracturing, a Steady-State Thermal analysis followed by a Static Structural analysis has been conducted. The axial displacement on the upper and lower bounds of the whole model and the radial displacement on the outer boundary of formation are all set to be zero. Furthermore, 70 MPa net increased casing pressure is exerted on the inner boundary of casing. The initial temperature is uniform at 100 °C on the whole model and it decreased to 30 °C on the casing inner wall while still maintaining 100 °C on the formation outer wall during fracturing.
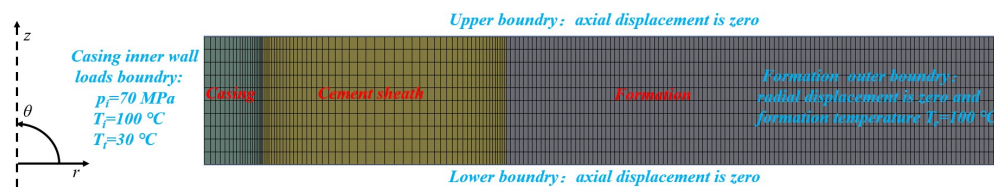
Figure 3. The 2D axisymmetric finite element analysis model of casing-cement sheath-formation system.

Figure 4 shows the comparison of cement sheath stresses between analytical model results and finite element analysis ones. It can be seen that the radial stress, tangential stress, and axial stress in the cement sheath calculated with two methods are all very close. The average relative errors of three kinds of stress are 7%, 5%, and 2% respectively, which indicated that the proposed model can be applicable for cement sheath stress calculation during fracturing to some extent.
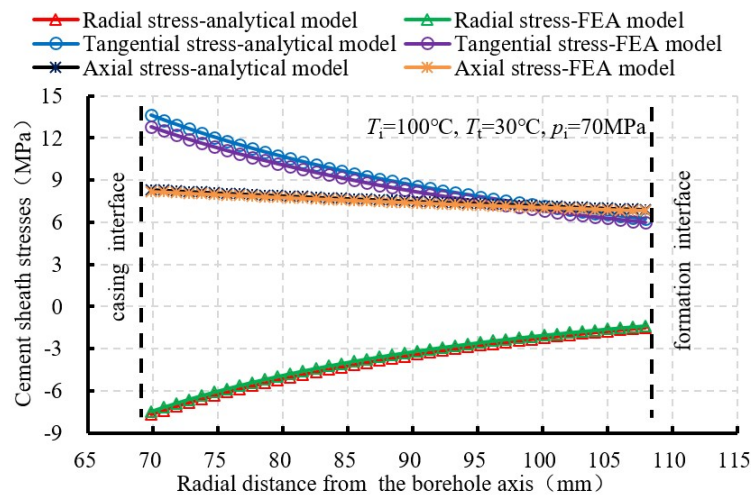

Figure 4. Comparison of stresses calculated with the analytical model and the finite element analysis model.

3.2.2. De-Bonding

De-bonding occurs when radial tensile stress at the cement interfaces exceeds its own tensile strength, which may mainly result from decreased wellbore temperature during fracturing fluid injection [19]. Figure 5 shows the radial distribution of the radial stress in the cement sheath considering increased casing pressure p_i of 0–70 MPa and decreased temperature at the casing inner wall of 70 °C. It can be seen from Figure 5 that the decreased wellbore temperature will induce significant radial

tensile stress, which is very harmful to cement sheath and may cause de-bonding. However, the increased casing pressure will produce radial compressed stress in the cement sheath at the same time and offset the radial tensile stress. In addition, with the increase of casing pressure p_i, the radial stress in the cement sheath gradually changes from tensile to compressed stress, which indicates that the risk of de-bonding decreases. When the increased casing pressure is 50 MPa, the radial stress is nearly compressive. Consequently, maintaining higher circulation pumping pressures, avoiding pumping off during injection, and lowering the pump pressure slowly during the operation completion will all be beneficial for cement sheath protection.
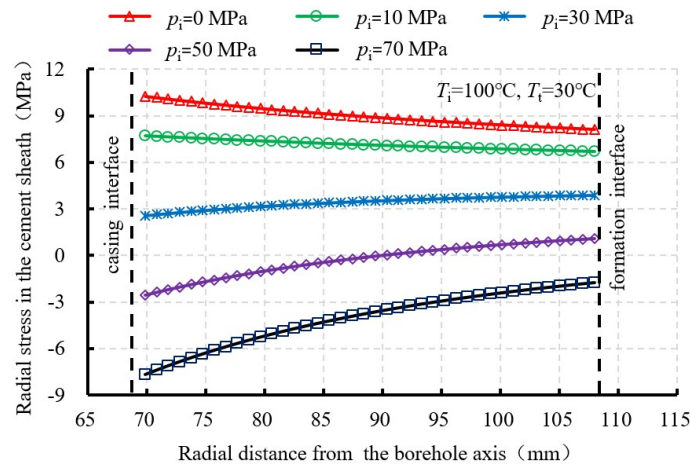
Figure 5. Radial distribution of the radial stress in the cement sheath under different increased casing pressures p_i and a decreased temperature of 70 °C at the casing inner wall.

Figure 6 shows the safety factors of cement sheath for de-bonding at two interfaces under different increased casing pressures p_i. It can be seen form Figure 6 that the safety factors at the casing-cement interface and the cement-formation interface both increase exponentially with the increase of casing pressure p_i. When p_i is less than 32 MPa, both interfaces will separate. When p_i is between 32 MPa and 42 MPa, only the cement-formation interface will separate. When p_i is larger than 42 MPa, both interfaces will not separate. Generally, the outer de-bonding is more relatively easy compared to inner de-bonding. This is because increased casing pressure p_i has a larger effect on the casing-cement interface. For the integrity of cement sheath, the value of p_i must be maintained above 42 MPa during the whole fracturing fluid injection stage.
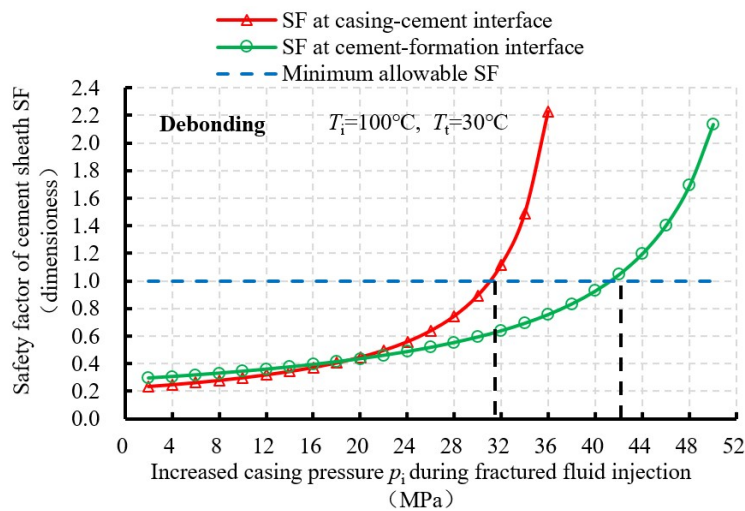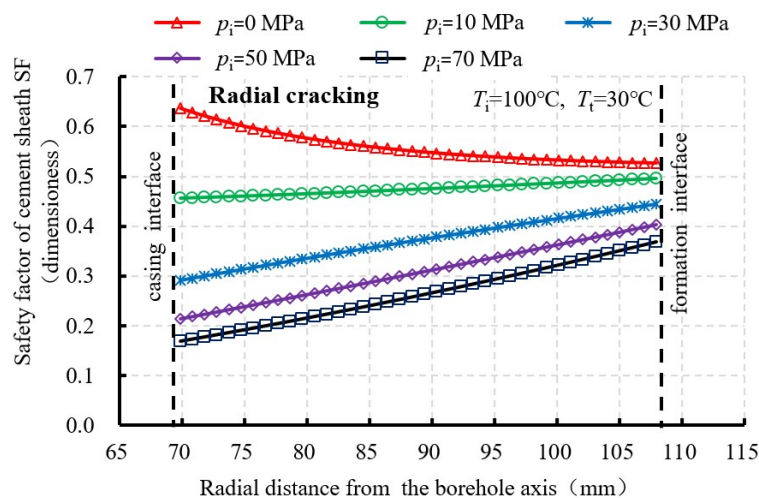

Figure 6. Safety factor of cement sheath for de-bonding at two interfaces under different increased casing pressures p_i and decreased temperature of 70 °C at the casing inner wall.

3.2.3. Radial Cracking

Radial cracking appears when tangential tensile stress in the cement surpasses its own tensile strength, Figures 7 and 8 shows the radial distribution of the tangential stress and safety factors for radial cracking in the cement sheath considering increased casing pressure p_i of 0–70 MPa and decreased temperature at the casing inner wall of 70 °C. It can be seen from Figure 7 that the decreased wellbore temperature and increased casing pressure will both induce significant tangential tensile stress, which leads to the risk of radial cracking. Figure 8 shows that the safety factors are all less than one under the present operation parameters, which means that radial cracking occurs completely. To some extent, this answers for the sustaining annular pressure after gas production. Meanwhile, we can also know easily that the maximum tangential tensile stress is nearly located at the casing-cement sheath interface and is caused by a decreased temperature of 70 °C, which is nearly 10 MPa less than that caused by increased casing pressure of 70 MPa. This indicates that radial cracking is mainly induced by increased casing pressure p_i and it occurs from the inner wall to the outer wall. However, p_i cannot be reduced during fracturing fluid injection because the need of fracture generation. Consequently, some other measures must be taken for protecting cement sheath, such as selecting cement with low elasticity and high tensile strength.
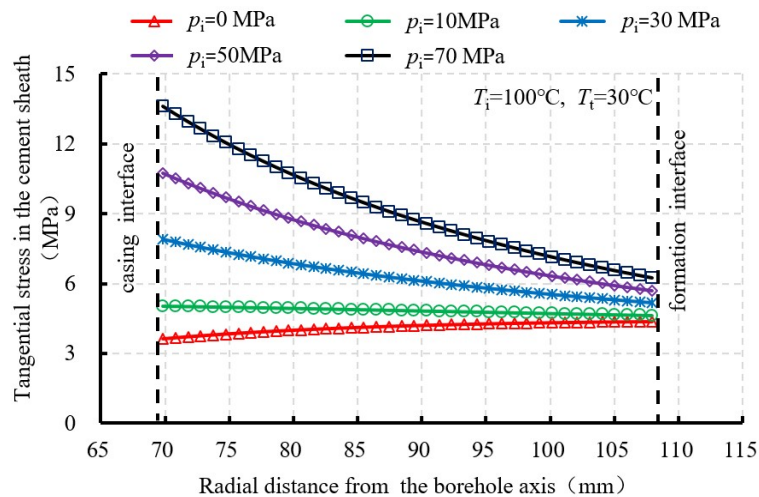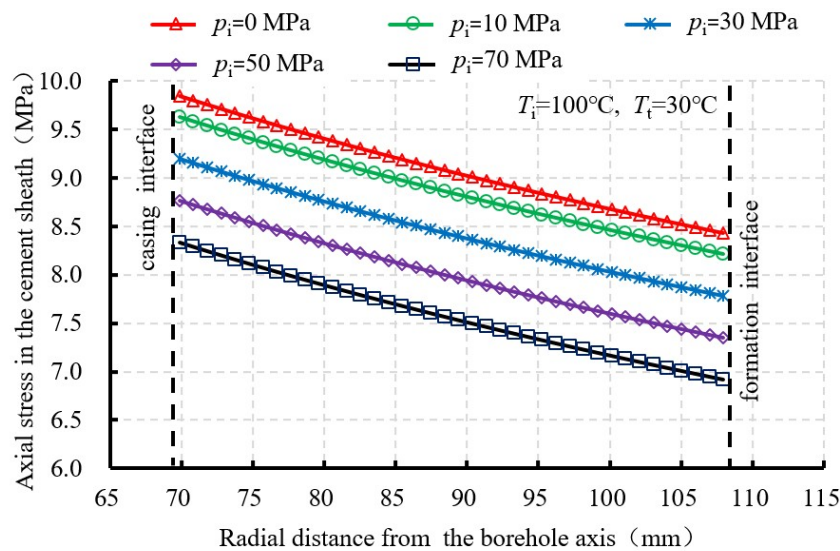

Figure 7. Radial distribution of the tangential stress in the cement sheath under different increased casing pressure p_i and decreased temperature of 70 °C at the casing inner wall.
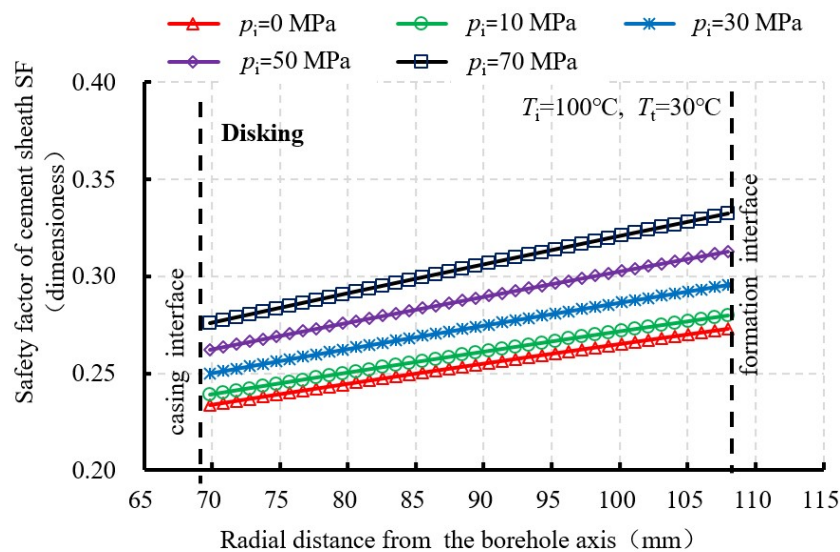

Figure 8. Radial distribution of the cement sheath safety factors for radial cracking under different increased casing pressures p_i and decreased temperature of 70 °C at the casing inner wall.

3.2.4. Disking

Disking occurs when axial tensile stress in the cement sheath exceeds its tensile strength when the gas leaking will run across the cement wall. Figures 9 and 10 show, respectively, the radial distribution of the axial stress and safety factors for disking in the cement sheath considering increased casing pressure p_i of 0–70 MPa and decreased temperature at the casing inner wall of 70 °C. It can be seen from Figure 9 that the decreased wellbore temperature will induce significant axial tensile stress, which may cause disking and is very threatening for cement sheath. Yet, the increased casing pressure will produce axial compressed stress and offset a portion of the axial tensile stress but is very limited. Figure 10 shows that the safety factors for disking are all less than one under the present operation parameters, which indicates that disking occurs through the cement sheath. This is also the reason for sustaining annular pressure. Taking Figures 9 and 10 into consideration simultaneously, it can be found that disking mainly results from the decreased wellbore temperature and it will generate from the inner wall to the outer wall. Consequently, increasing the temperature of injected fracturing fluid can reduce the risk of disking.
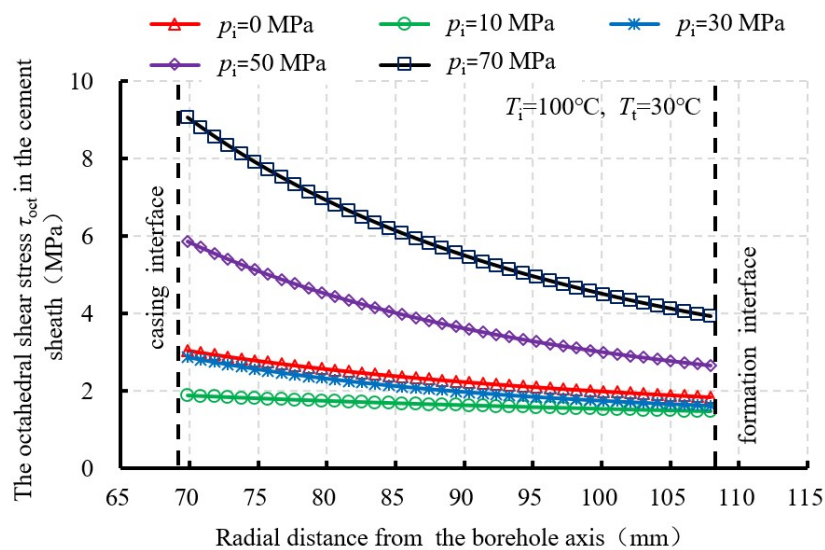

Figure 9. Radial distribution of the axial stress in the cement sheath under different increased casing pressures p_i and a decreased temperature of 70 °C at the casing inner wall.
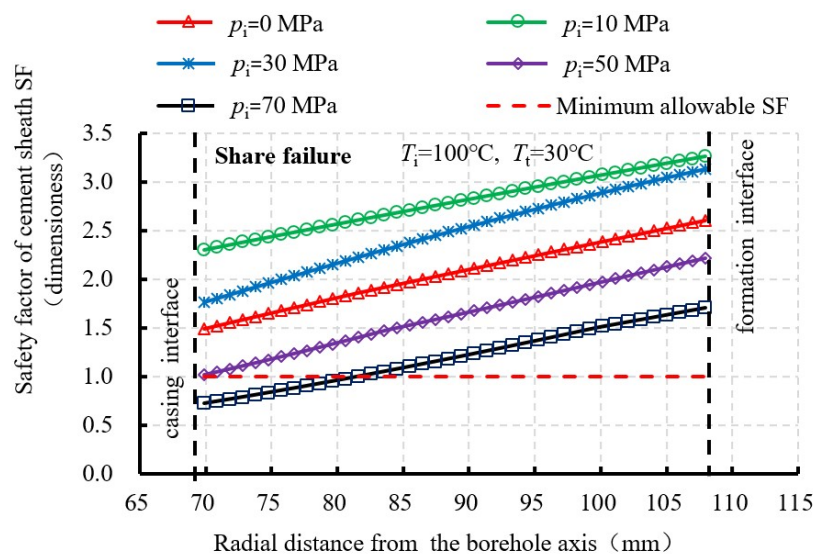

Figure 10. Radial distribution of the cement sheath safety factors for disking under different increased casing pressures p_i and a decreased temperature of 70 °C at the casing inner wall.

3.2.5. Shear Failure

Shear failure generally causes the entire failure of cement sheath. Figures 11 and 12 show the radial distribution of the octahedral shear stress and safety factors for shear failure in the cement sheath considering increased casing pressure p_i of 0–70 MPa and decreased temperature at the casing inner wall of 70 °C. It can be seen from Figure 11 that the decreased wellbore temperature and increased casing pressure induce significant octahedral shear stress. When the decreased temperature at the casing inner wall is 70 °C with the increase of p_i, the octahedral shear stress τ_{oct} decreases first and then increases. The maximum τ_{oct} is located at the casing interface. From Figure 12, we can conclude that the shear failure of cement sheath nearly does not occur if the increased casing pressure p_i is less than 50 MPa while the shear failure will initiate from the inner wall to the outer wall. Considering the present operation parameters, some measures must be taken, such as selecting cement with low elasticity, for protecting cement sheath.
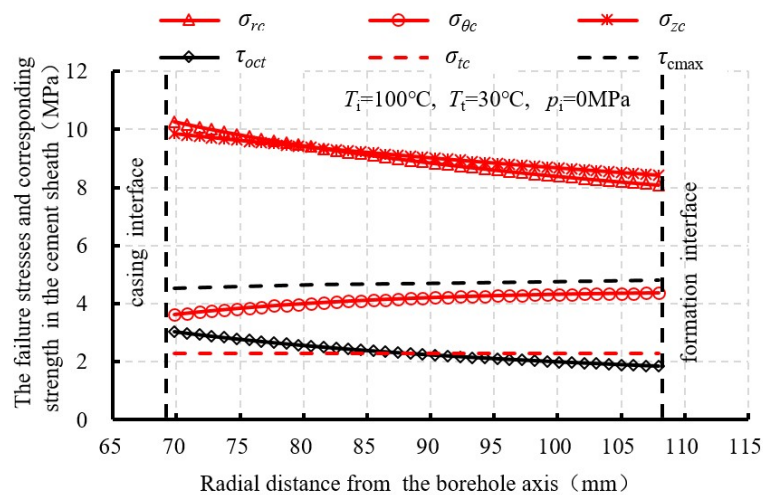

Figure 11. Radial distribution of the octahedral shear stress τ_{oct} in the cement sheath under different increased casing pressures p_i and a decreased temperature of 70 °C at the casing inner wall.
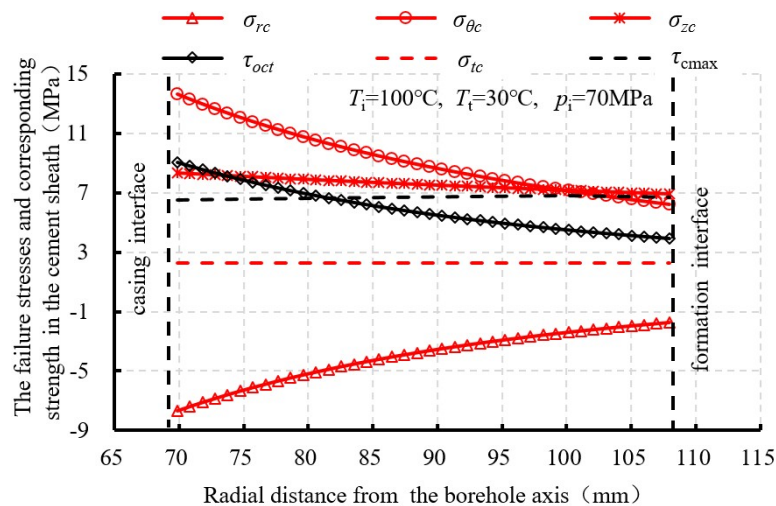

Figure 12. Radial distribution of the cement sheath safety factors for shear failure under different increased casing pressures p_i and a decreased temperature of 70 °C at the casing inner wall.

3.3. Comparison and Discussion

Figures 13 and 14 show the radial distribution of the failure stress and corresponding strength in the cement sheath considering increased casing pressure p_i of 0 or 70 MPa and decreased temperature at the casing inner wall of 70 °C, respectively. It can be seen from Figure 13 that the decreased wellbore temperature has produced significant tri-axial tensile stress in the cement sheath and three of them exceed its own tensile strength, which will induce cement failure of de-bonding, radial cracking, and disking, especially de-bonding and disking. While the octahedral shear stress is less than the maximum allowable shear stress for cement sheath, it shows that shear failure will not appear. Consequently, increasing properly the injected fluid temperature can lower the failure risks of cement sheath for fracturing wells.

Figure 13. Radial distribution of the failure stress and corresponding strength of the cement sheath under only a decreased temperature of 70 °C at the casing inner wall.
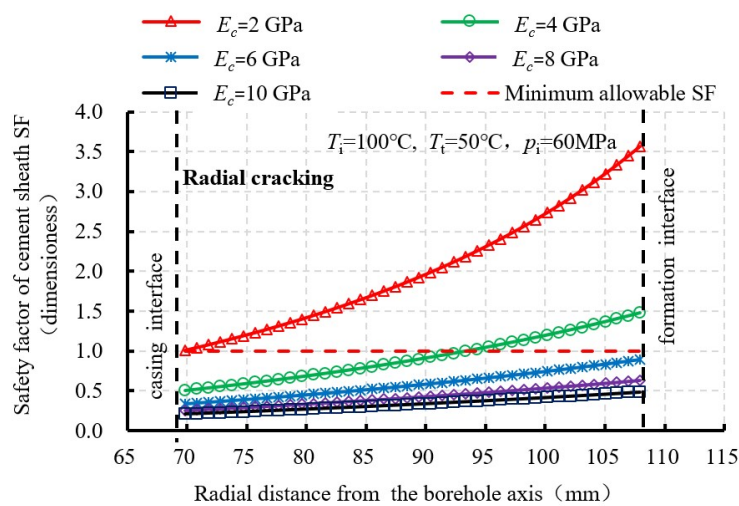

Figure 14. Radial distribution of the failure stress and corresponding strength of the cement sheath under an increased casing pressure p_i of 70 MPa and a decreased temperature of 70 °C at the casing inner wall.

Figure 14 shows that, when considering the increased casing pressure p_i of 70 MPa simultaneously, the radial stress has turned into compressive but tangential and axial stresses, which are still tensile and still clearly larger than the tensile strength of cement sheath, which will lead to cement failure of radial cracking and disking. Meanwhile, the octahedral shear stress has also exceeded the maximum allowable shear stress near the casing interface, which indicates that shear failure occurs at this location.

Combining the analysis above, we know that the increased casing pressure will significantly lower the de-bonding risk but aggravate radial cracking and shear failure. For protecting cement sheath integrity, higher circulation pumping pressures should be maintained in order to avoid de-bonding during whole fracturing operations.

In order to lower the risks of radial cracking, disking, and shear failure for cement sheath under a high pumping pressure from fracturing, the common method is cemented with low elasticity modulus cement sheath. Figures 15–17 show, respectively, the radial distribution of the cement sheath safety factors for three kinds of failure modes under a different elasticity modulus of cement sheath E_c. The considered increased casing pressure p_i is 60 MPa and the decreased temperature at the casing inner wall is 50 °C. It can be seen from Figures 15–17 that, with a decrease of E_c, three kinds of safety factors increase gradually and the increasing range is larger and larger. Therefore, lowering the elasticity modulus of cement sheath is very effective for cement protection. When E_c is about lower than 4 GPa, cement sheath will not occur to radial cracking and disking. Meanwhile, when E_c is about lower than 8 GPa, the shear failure may not occur. In conclusion, cement sheath with a low elasticity modulus must be adopted in fracturing wells.

Figure 15. Radial distribution of the cement sheath safety factors for radial cracking under a different elasticity modulus of cement sheath.
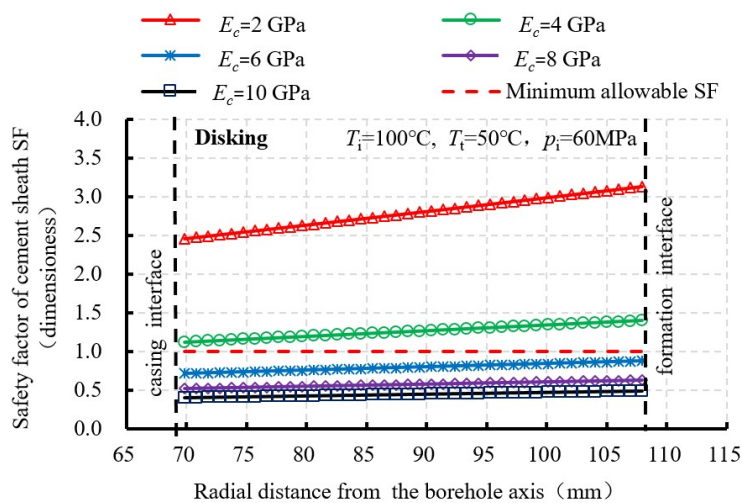
Figure 16. Radial distribution of the cement sheath safety factors for disking under a different elasticity modulus of cement sheath.
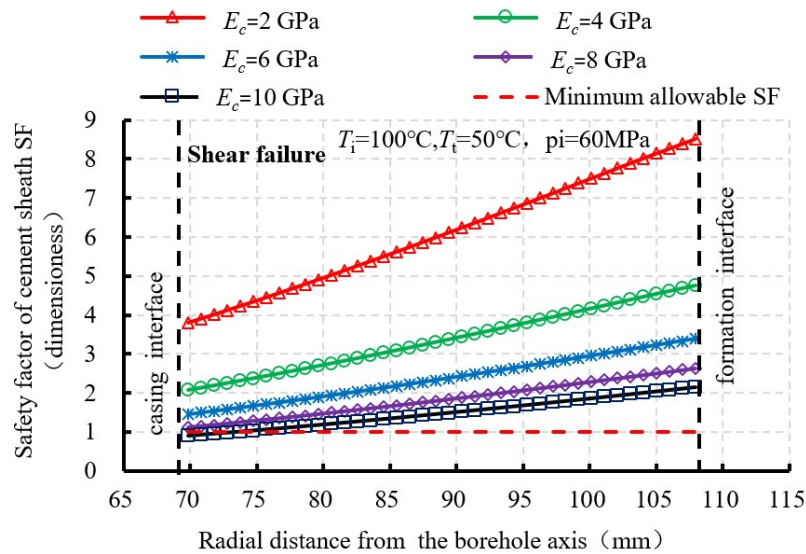
Figure 17. Radial distribution of the cement sheath safety factors for shear failure under a different elasticity modulus of cement sheath.

4. Conclusions

(1)　The radial distributions of failure stresses and corresponding safety factors for cement sheath have been analyzed under four failure modes, including de-bonding, radial cracking, disking, and shear failure.

(2)　The decreased wellbore temperature will produced significant tri-axial tensile stress and induce cement failure of de-bonding, radial cracking, and disking.

(3)　The increased casing pressure will significantly lower the risk of de-bonding but also aggravate radial cracking and shear failure.

(4)　Increasing the injected fluid temperature, maintaining a higher circulation pumping pressures and adopting cement sheath with a low elasticity modulus can protect cement sheath in fracturing wells.

(5)　Considering some assumptions before model development, some conclusions may not be entirely appropriate. Further model improvement including casing centralization, anisotropy of the formation stresses, and a transient wellbore temperature change should be investigated.

List of Symbols

$\sigma_r^T, \sigma_\theta^T, \sigma_z^T$	Radial, tangential, and axial thermal stress of cylinder, respectively, MPa
$\sigma_r^P, \sigma_\theta^P, \sigma_z^P$	Radial, tangential, and axial stress of cylinder caused by increased inner pressure, respectively, MPa
$\sigma_{rs}^T, \sigma_{\theta s}^T, \sigma_{zs}^T$	Radial, tangential, and axial thermal stress of casing, respectively, MPa
$\sigma_{rc}^T, \sigma_{\theta c}^T, \sigma_{zc}^T$	Radial, tangential, and axial thermal stress of cement sheath, respectively, MPa
$\sigma_{rf}^T, \sigma_{\theta f}^T, \sigma_{zf}^T$	Radial, tangential, and axial thermal stress of formation, respectively, MPa
$\sigma_{rs}^P, \sigma_{\theta s}^P, \sigma_{zs}^P$	Radial, tangential, and axial stress of casing caused by increased casing pressure, respectively, MPa
$\sigma_{rc}^P, \sigma_{\theta c}^P, \sigma_{zc}^P$	Radial, tangential, and axial stress of cement sheath caused by increased casing pressure, respectively, MPa
$\sigma_{rf}^P, \sigma_{\theta f}^P, \sigma_{zf}^P$	Radial, tangential, and axial stress of formation caused by increased casing pressure, respectively, MPa
$\sigma_{rc}, \sigma_{\theta c}, \sigma_{zc}$	Combined radial, tangential, and axial stress of cement sheath caused by decreased wellbore temperature and increased casing pressure during fracturing fluid injection, respectively, MPa
$\sigma_1, \sigma_2, \sigma_3$	Maximum, intermediate, and minimum principal stresses in the cement sheath, respectively, MPa
u^T	Radial thermal displacement in the cylinder, mm
u^P	Radial displacement in the cylinder caused by increased inner pressure, mm
u_s^T, u_c^T, u_f^T	Radial thermal displacement for casing, cement sheath, and formation, respectively, mm
u_s^P, u_c^P, u_f^P	Radial displacement caused by increased casing pressure for casing, cement sheath, and formation, respectively, mm
E, E_s, E_c, E_f	Elasticity modulus of ordinary cylinder, casing, cement sheath, and formation, respectively, MPa
μ, μ_s, μ_c, μ_f	Poisson's ratio of ordinary cylinder, casing, cement sheath, and formation, respectively, dimensionless
$\alpha, \alpha_s, \alpha_c, \alpha_f$	Linear thermal expansion coefficient of ordinary cylinder, casing, cement sheath, and formation, respectively, 1/°C
a	Internal radius of thick wall cylinder, mm
r	Radial distance from the axis of wellbore, mm
r_i	Inside radius of casing, mm
r_1	Outside radius of casing or inside radius of cement sheath, mm
r_2	Outside radius of cement sheath or inside radius of formation, mm
r_o	Outside radius of formation, mm
$T(r)$	Temperature change value at the radius of r after fracturing fluid injection, °C
T_i	Wellbore temperature before fracturing fluid injection, °C
T_t	Wellbore temperature after fracturing fluid injection, °C
T_e	Formation temperature, °C
$C_1, C_{1s}, C_{1c}, C_{1f}$	Undetermined coefficients, dimensionless
$C_2, C_{2s}, C_{2c}, C_{2f}$	Undetermined coefficients, m^2
$[A], \{B\}$	Coefficient matrix and constant vector for Equation (A5), respectively
σ_{tc}	Tensile strength of cement sheath, MPa
σ_{cc}	Uniaxial compressive strength of cement sheath, MPa
$\tau_{c\max}$	The maximum allowable shear stress for cement sheath, MPa
τ_{oct}	Octahedral shear stress, MPa
c_c	Cohesion of cement sheath, MPa
ϕ_c	Angle of internal friction of cement sheath, (°)
p_i	Increased casing pressure, MPa
p_{c1}	Contact pressure at the casing-cement sheath interface induced by increased casing pressure, MPa
p_{c2}	Contact pressure at the cement sheath-formation interface induced by increased casing pressure, MPa
p_f	Changed formation pressure, MPa
SF	Safety factor of cement sheath, dimensionless

Appendix A. Cement Sheath Stress Induced by a Decrease of Wellbore Temperature

Submitting Equations (2) and (3) into Equation (1), the thermal radial displacement and thermal stresses for the combined system can be determined and the detailed derivative results are given below [12].

For the casing ($r_i \leq r \leq r_1$):

$$
\begin{cases}
u_s^T = \frac{1+\mu_s}{1-\mu_s}\frac{\alpha_s}{r}\frac{1}{2}(T_t - T_i)(r^2 - r_i^2) + C_{1s}r + \frac{C_{2s}}{r} \\[2mm]
\sigma_{rs}^T = -\frac{\alpha_s E_s}{1-\mu_s}\frac{1}{r^2}\frac{1}{2}(T_t - T_i)(r^2 - r_i^2) + \frac{E_s}{1+\mu_s}\left(\frac{C_{1s}}{1-2\mu_s} - \frac{C_{2s}}{r^2}\right) \\[2mm]
\sigma_{\theta s}^T = \frac{\alpha_s E_s}{1-\mu_s}\frac{1}{r^2}\frac{1}{2}(T_t - T_i)(r^2 - r_i^2) - \frac{\alpha_s E_s (T_t - T_i)}{1-\mu_s} + \frac{E_s}{1+\mu_s}\left(\frac{C_{1s}}{1-2\mu_s} + \frac{C_{2s}}{r^2}\right) \\[2mm]
\sigma_{zs}^T = -\frac{\alpha_s E_s (T_t - T_i)}{1-\mu_s} + \frac{2\mu_s E_s C_{1s}}{(1+\mu_s)(1-2\mu_s)}
\end{cases}
\tag{A1}
$$

For the cement sheath ($r_1 \leq r \leq r_2$):

$$
\begin{cases}
u_c^T = \frac{1+\mu_c}{1-\mu_c}\frac{\alpha_c}{r}\left\{\frac{T_t-T_i}{2}(r^2-r_1^2) + \frac{(T_i-T_t)}{2\ln(r_o/r_1)}\left[r^2\ln\left(\frac{r}{r_1}\right) - \frac{r^2}{2} + \frac{r_1^2}{2}\right]\right\} + C_{1c}r + \frac{C_{2c}}{r} \\[2mm]
\sigma_{rc}^T = -\frac{\alpha_c E_c}{1-\mu_c}\frac{1}{r^2}\left\{\frac{T_t-T_i}{2}(r^2-r_1^2) + \frac{(T_i-T_t)}{2\ln(r_o/r_1)}\left[r_1\ln\left(\frac{r}{r_1}\right) - \frac{r^2}{2} + \frac{r_1^2}{2}\right]\right\} + \frac{E_c}{1+\mu_c}\left(\frac{C_{1c}}{1-2\mu_c} - \frac{C_{2c}}{r^2}\right) \\[2mm]
\sigma_{\theta c}^T = \frac{\alpha_c E_c}{1-\mu_c}\frac{1}{r^2}\left\{\frac{T_t-T_i}{2}(r^2-r_1^2) + \frac{(T_i-T_t)}{2\ln(r_o/r_1)}\left[r^2\ln\left(\frac{r}{r_1}\right) - \frac{r^2}{2} + \frac{r_1^2}{2}\right]\right\} \\[2mm]
\quad - \frac{\alpha_c E_c}{1-\mu_c}\left[T_t - T_i + (T_i - T_t)\frac{\ln(r/r_1)}{\ln(r_o/r_1)}\right] + \frac{E_c}{1+\mu_c}\left(\frac{C_{1c}}{1-2\mu_c} + \frac{C_{2c}}{r^2}\right) \\[2mm]
\sigma_{zc}^T = -\frac{\alpha_c E_c}{1-\mu_c}\left[T_t - T_i + (T_i - T_t)\frac{\ln(r/r_1)}{\ln(r_o/r_1)}\right] + \frac{2\mu_c E_c C_{1c}}{(1+\mu_c)(1-2\mu_c)}
\end{cases}
\tag{A2}
$$

For the formation ($r_2 \leq r \leq r_o$):

$$
\begin{cases}
u_f^T = \frac{1+\mu_f}{1-\mu_f}\frac{\alpha_f}{r}\left\{\frac{T_t-T_i}{2}(r^2-r_1^2) + \frac{(T_i-T_t)}{2\ln(r_o/r_1)}\left[r^2\ln(r/r_1) - \frac{r^2}{2} + \frac{r_1^2}{2}\right]\right\} + C_{1f}r + \frac{C_{2f}}{r} \\[2mm]
\sigma_{rf}^T = -\frac{\alpha_f E_f}{1-\mu_f}\frac{1}{r^2}\left\{\frac{T_t-T_i}{2}(r^2-r_1^2) + \frac{(T_i-T_t)}{2\ln(r_o/r_1)}\left[r^2\ln(r/r_1) - \frac{r^2}{2} + \frac{r_1^2}{2}\right]\right\} + \frac{E_f}{1+\mu_f}\left(\frac{C_{1f}}{1-2\mu_f} - \frac{C_{2f}}{r^2}\right) \\[2mm]
\sigma_{\theta f}^T = \frac{\alpha_f E_f}{1-\mu_f}\frac{1}{r^2}\left\{\frac{T_t-T_i}{2}(r^2-r_1^2) + \frac{(T_i-T_t)}{2\ln(r_o/r_1)}\left[r^2\ln(r/r_1) - \frac{r^2}{2} + \frac{r_1^2}{2}\right]\right\} \\[2mm]
\quad - \frac{\alpha_f E_f}{1-\mu_f}\left[T_t - T_i + (T_i - T_t)\frac{\ln(r/r_1)}{\ln(r_o/r_1)}\right] + \frac{E_f}{1+\mu_f}\left(\frac{C_{1f}}{1-2\mu_f} + \frac{C_{2f}}{r^2}\right) \\[2mm]
\sigma_{zf}^T = -\frac{\alpha_f E_f}{1-\mu_f}\left[T_t - T_i + (T_i - T_t)\frac{\ln(r/r_1)}{\ln(r_o/r_1)}\right] + \frac{2\mu_f E_f C_{1f}}{(1+\mu_f)(1-2\mu_f)}
\end{cases}
\tag{A3}
$$

Now, let us solve the six undetermined coefficients of C_{1s}, C_{2s}, C_{1c}, C_{2c}, C_{1f}, and C_{2f} in Equation (A1) to Equation (A3). Suppose the combined system is completely cemented at two interfaces. The boundary conditions and the continuity conditions of the radial thermal stress and thermal radial displacement at the two interfaces are as follows.

$$
\begin{cases}
\begin{cases}
\sigma_{rs}^T\big|_{r=r_i} = 0 \\[1mm]
\sigma_{rf}^T\big|_{r=r_o} = 0
\end{cases} \\[4mm]
\begin{cases}
\sigma_{rs}^T\big|_{r=r_1} = \sigma_{rc}^T\big|_{r=r_1} \\[1mm]
u_s^T\big|_{r=r_1} = u_c^T\big|_{r=r_1}
\end{cases} \\[4mm]
\begin{cases}
\sigma_{rc}^T\big|_{r=r_{21}} = \sigma_{rf}^T\big|_{r=r_{21}} \\[1mm]
u_c^T\big|_{r=r_2} = u_f^T\big|_{r=r_2}
\end{cases}
\end{cases}
\tag{A4}
$$

Then submitting Equations (A1) to (A3) into Equation (A4), we get the system of linear equations with unknown number of C_{1s}, C_{2s}, C_{1c}, C_{2c}, C_{1f}, and C_{2f} as follows.

$$
[A] \times \left\{C_{1s},\ C_{2s},\ C_{1c}, C_{2c}, C_{1f}, C_{2f}\right\}^T = \{B\}
\tag{A5}
$$

In Equation (A5), the coefficient matrix $[A]$ and constant vector $\{B\}$ can both be obtained from the final actual boundary and continuity conditions. The Gaussian main elimination method was selected for solving Equation (A5) [20]. Then, submitting C_{1c} and C_{2c} into Equation (A2), we can get the radial thermal displacement and thermal stress induced by a decrease of wellbore temperature during fracturing at any radius of r in the cement sheath.

References

1. Shadravan, A.; Schubert, J.; Amani, M.; Teodoriu, C. HPHT cement sheath integrity evaluation method for unconventional wells. In Proceedings of the SPE International Conference on Health, Safety, and Environment, Long Beach, CA, USA, 17–19 March 2014.
2. Wang, W.; Taleghani, A.D. Cement sheath integrity during hydraulic fracturing: An integrated modeling approach. In Proceedings of the SPE Hydraulic Fracturing Technology Conference, The Woodlands, TX, USA, 4–6 February 2014.
3. Vrålstad, T.; Skorpa, R.; Opedal, N.; Andrade, J.D. Effect of thermal cycling on cement sheath integrity: Realistic experimental tests and simulation of resulting leakages. In Proceedings of the SPE Thermal Well Integrity and Design Symposium, Banff, AB, Canada, 23–25 November 2015.
4. Thiercelin, M.J.; Dargaud, B.; Baret, J.F.; Rodriquez, W.J. Cement design based on cement mechanical response. *SPE Drill. Complet.* **1998**, *13*, 266–273. [CrossRef]
5. Jing, L.I.; Lin, C.Y.; Yang, S.C.; Zhi, Y.; Chen, S. Theoretical solution of thermal stress for casing-cement-formation coupling system. *J. China Univ. Pet.* **2009**, *33*, 63–69.
6. Li, Y.; Liu, S.; Wang, Z.; Yuan, J.; Qi, F. Analysis of cement sheath coupling effects of temperature and pressure in non-uniform in-situ stress field. In Proceedings of the International Oil and Gas Conference and Exhibition in China, Beijing, China, 8–10 June 2010.
7. Bois, A.P.; Garnier, A.; Galdiolo, G.; Laudet, J.B. Use of a mechanistic model to forecast cement-sheath integrity for CO_2 storage. In Proceedings of the SPE International Conference on CO_2 Capture, Storage, and Utilization, New Orleans, LA, USA, 10–12 November 2010.
8. Haider, M.G.; Sanjayan, J.; Ranjith, P.G. Modeling of a wellbore composite cylinder system for cement sheath stress analysis in geological sequestration of CO_2. In Proceedings of the 46th U.S. Rock Mechanics/Geomechanics Symposium, Chicago, IL, USA, 24–27 June 2012.
9. Bui, B.T.; Tutuncu, A.N. Modeling the failure of cement sheath in anisotropic stress field. In Proceedings of the SPE Unconventional Resources Conference Canada, Calgary, AB, Canada, 5–7 November 2013.
10. Xi, Y.; Li, J.; Liu, G.H.; Zha, C.Q.; Yan, P. Analysis on cement sheath integrity under transient thermo-mechanical coupling effect. *Oil Drill. Prod. Technol.* **2017**, *39*, 417–423.
11. Xu, H.; Zhang, Z.; Shi, T.; Xiong, J.Y. Influence of the WHCP on cement sheath stress and integrity in HTHP gas well. *J. Pet. Sci. Eng.* **2015**, *126*, 174–180.
12. Xu, H.; Peng, N.; Ma, T.; Yang, B. Investigation of thermal stress of cement sheath for geothermal wells during fracturing. *Energies* **2018**, *11*, 2581. [CrossRef]
13. Xu, B.; Wang, J. *Theory of Elastic Mechanics*; Tsinghua University Press: Beijing, China, 2007.
14. Bois, A.P.; Garnier, A.; Galdiolo, G.; Laudet, J.B. Use of a mechanistic model to forecast cement-sheath integrity. *SPE Drill. Complet.* **2012**, *27*, 303–314. [CrossRef]
15. Al-Ajmi, A.M.; Zimmerman, R.W. Relation between the Mogi and the Coulomb failure criteria. *Int. J. Rock Mech. Min. Sci.* **2005**, *42*, 431–439. [CrossRef]
16. Ma, T.S.; Chen, P.; Yang, C.H.; Zhao, J. Wellbore stability analysis and well path optimization based on the breakout width model and Mogi-Coulomb criterion. *J. Pet. Sci. Eng.* **2015**, *135*, 678–701. [CrossRef]
17. Nelson, E.B.; Guillot, D. *Well Cementing*, 2nd ed.; Schlumberger: Amsterdam, The Netherlands, 2006.
18. Jaeger, J.C.; Cook, N.G.W.; Zimmerman, R.W. *Fundamentals of Rock Mechanics*, 4th ed.; Blackwell Publishing: Hoboken, NJ, USA, 2007.
19. Andrade, J.D. Cement Sheath Integrity during Thermal Cycling. Ph.D. Thesis, Norwegian University of Science and Technology, Trondheim, Norway, 2015.
20. Li, Q.; Wang, N. *Numerical Analysis*; Tsinghua University Press: Beijing, China, 2008.